Available online at www.sciencedirect.com
SCIENCE DIRECT®

Journal of the European Ceramic Society 24 (2004) 3409–3417
www.elsevier.com/locate/jeurceramsoc

Si/B/C/N/Al precursor-derived ceramics: Synthesis, high temperature behaviour and oxidation resistance

A. Müller[a,*], P. Gerstel[a], E. Butchereit[b], K.G. Nickel[b], F. Aldinger[a]

[a] *Max-Planck-Institut für Metallforschung and Institut für Nichtmetallische Anorganische Materialien, Universität Stuttgart, Pulvermetallurgisches Laboratorium, Heisenbergstr. 3, D-70569 Stuttgart, Germany*

[b] *Eberhard-Karls-Universität Tübingen, Institut für Geowissenschaften, Wilhelmstr. 56, D-72074 Tübingen, Germany*

Abstract

The Si/B/C/N/H polymer T2(1), $[B(C_2H_4Si(CH_3)NH)_3]_n$, was reacted with different amounts of $H_3Al{\cdot}NMe_3$ to produce three organometallic precursors for Si/B/C/N/Al ceramics. These precursors were transformed into ceramic materials by thermolysis at 1400 °C. The ceramic yield varied from 63% for the Al-poor polymer (3.6 wt.% Al) to 71% for the Al-rich precursor (9.2 wt.% Al). The as-thermolysed ceramics contained nano-sized SiC crystals. Heat treatment at 1800 °C led to the formation of a microstructure composed of crystalline SiC, Si_3N_4, AlN(+SiC) and a BNC_x phase. At 2000 °C, nitrogen-containing phases (partly) decomposed in a nitrogen or argon atmosphere. The high temperature stability was not clearly related to the aluminium concentration within the samples. The oxidation behaviour was analysed at 1100, 1300, and 1500 °C. The addition of aluminium significantly improved the oxide scale quality with respect to adhesion, cracking and bubble formation compared to Al-free Si(/B)/C/N ceramics. Scale growth rates on Si/B/C/N/Al ceramics at 1500 °C were comparable with CVD–SiC and CVD–Si_3N_4, which makes these materials promising candidates for high-temperature applications in oxidizing environments.

Keywords: Oxidation; Precursor-derived ceramics; Precursors-organic; Si–B–C–N–Al; Synthesis

1. Introduction

In the past years, a number of precursors for the preparation of precursor-derived ceramics in the system Si/B/C/N/(O) have been investigated. By means of various spectroscopic techniques, the structures of the polymeric precursors and the resulting ceramics have been solved.[1,2] Together with thermogravimetric analysis (TGA) and Transmission Electron Microscopy (TEM) this has given insight into the cross-linking and ceramization mechanisms.[3,4] Based upon this knowledge, it is nowadays conceivable to prepare ceramic materials with tailored microstructures and—to a certain extend—tailored thermal and mechanical properties. By incorporation of boron into Si/C/N ceramics, the high temperature behaviour may change drastically. Many Si/B/C/N precursor-derived materials exhibit an extraordinary high temperature stability against crystallization and decomposition.[5–7]

As for polymers, a variety of shaping techniques are available, which allow the preparation of fibres and monoliths, as well as oxidation resistant coatings.[7,8] In addition, precursor solutions can be used to infiltrate porous materials.[9] The variety of different shapes together with interesting functional and structural properties of these materials open a broad field of possible technical applications. Many of these include the use in oxidizing high-temperature environments. Determination of the oxidation resistance is, therefore, of importance.

Systematic investigations of the oxidation behaviour of precursor-derived ceramics in the system Si/(B)/C/N have been reported by the authors previously.[10] They found a good oxidation resistance of both, boron-free and boron-containing samples, with that of the latter being comparable to CVD–SiC and CVD–Si_3N_4. It is striking that boron-containing ceramics showed amorphous oxide scales after oxidation at 1500 °C for up to 24 h. On the contrary, cristobalite scales formed on precursor-derived Si/C/N ceramics as well as on CVD–SiC and CVD–Si_3N_4 under the same conditions.[11] Although the role of boron during oxidation of precursor-derived ceramics is not yet entirely understood, (partial) incorporation of boron into the scales seems responsible for the observed differences. However, at high temperatures boron tends to form volatile species.

* Corresponding author. Tel.: +49-711-689-3226.
E-mail address: amueller@aldix.mpi-stuttgart.mpg.de (A. Müller).

0955-2219/$ - see front matter © 2003 Elsevier Ltd. All rights reserved.
doi:10.1016/j.jeurceramsoc.2003.10.018

From literature it is known that oxidation of B_4C up to 1100 °C leads to the formation of protective B_2O_3 scales. In TGA, mass increases are observed. At higher oxidation temperatures, significant mass losses are measured due to volatilisation of B_2O_3.[12] In the case of precursor-derived Si/B/C/N ceramics, oxidation times exceeding 24 h at 1500 °C led to crystallisation of the formerly amorphous scales with concurrent bubble formation.[10] It is assumed that volatilisation of boron species is responsible for this behaviour. Similar observations were reported from the high-temperature oxidation of sintered SiC containing boron as a sintering additive. At 1500 °C, bubble formation was observed, with the number of bubbles increasing with increasing boron content.[13]

In this paper we report about synthesis, ceramization, thermal stability, and oxidation resistance of a new group of aluminium containing precursor-derived ceramics. The addition of aluminium mainly aimed at an improvement of the oxidation resistance. Volatilisation of boron and concurrent bubble formation should be impeded by formation of boron mullites and/or Al_2O_3/B_2O_3/SiO_2 glasses. In addition, an improvement of the scale quality with respect to cracking and spallation was expected.

2. Experimental part

2.1. Precursor synthesis and characterization

Precursor synthesis was carried out in a purified argon atmosphere using standard Schlenk techniques. Toluene solutions of the polymer T2(1) $[B(C_2H_4Si(CH_3)NH)_3]_n$ were obtained according to the literature: dichloromethylvinylsilane (ABCR chemicals) was hydroborated with $H_3B{\cdot}SMe_2$ (2 M solution in toluene, Sigma-Aldrich, Germany) in dry toluene and subsequently reacted with ammonia.[6] In contrast to the literature, ammonolysis was performed in dry toluene at about 60 °C (instead of THF at 0 °C) to obtain T2(1) molecules with a low molecular weight, which remain in solution. After filtration of NH_4Cl, the solution was concentrated under reduced pressure to yield a T2(1) content of about 12 wt.%. $H_3Al{\cdot}NMe_3$ was synthesized by reaction of $LiAlH_4$ with $Me_3N{\cdot}HCl$ (each Merck Eurolab GmbH, Germany) in dry Et_2O.[14]

In a typical experiment, 82 g of a T2(1) solution (12.2 wt.% in toluene, 10.0 g T2(1), 37 mmol) were used. A solution of $H_3Al{\cdot}NMe_3$ in 40 ml of toluene was added dropwise at room temperature whereby gas evolution was observed. The amounts of $H_3Al{\cdot}NMe_3$ used for the synthesis of **1**, **2**, and **3** were 3.3 g (37 mmol), 2.2 g (25 mmol), and 1.1 g (12 mmol), respectively. After complete addition of the alane, the mixture was stirred for 3 h at room temperature and subsequently heated to reflux for 3 h. The solvent was removed under reduced pressure and the residue was dried in vacuum (5×10^{-2} mbar) at 60 °C to produce a colourless air and moisture sensitive polymer in about 95% yield.

For the production of warm-pressed green bodies, the raw materials have to be cross-linked. They were heated to 250 °C for 1 h in an argon atmosphere followed by 15 min at 350 °C in a vacuum. This treatment yielded 85% of cross-linked polymer. After milling (WC ball mill) and sieving (<80 μm), about 0.2 g of the powder was filled into a cylindrical graphite mould (2.5 cm diameter) and warm-pressed uniaxially at 400 °C, 38.8 MPa for 1 h. The thickness of the obtained glassy greenbody was 0.4 mm.

Fourier Transform infrared spectra were obtained with a Bruker IFS 66 spectrometer as KBr pellets. Microanalysis was performed using a combination of different equipment (Elementar Vario EL, Eltra CS 800 C/S Determinator, Leco TC-436 N/O Determinator) and by atom emission spectrometry (ISA Jobin Yvon JY70 Plus).

2.2. Ceramization and heat treatment

Thermogravimetric analysis (TGA) of the polymer-to-ceramic conversion was performed in a flowing argon atmosphere (40 cm^3/min) with Netzsch STA 409 equipment in alumina crucibles (heating rate, 5 °C/min; 25–1400 °C). Bulk ceramization of the polymers was carried out in alumina Schlenk tubes in a flowing argon atmosphere. For the production of unshaped ceramic particles, polymers as obtained after synthesis were used (25–1400 °C; heating rate, 1 °C/min, dwell time 2 h). Ceramic monoliths were produced by thermolysis of warm-pressed greenbodies (1 °C/min to 500 °C, dwell time 12 h, 10 °C/h to 1000 °C, dwell time 1 h). For high temperature TGA experiments, as-obtained ceramic particles were heated to 2150 °C [heating rates, 10 °C/min (25–1400 °C) and 5 °C/min (1400–2150 °C)] in carbon crucibles in an argon atmosphere using Netzsch STA 501 equipment. Crystallization experiments of as-obtained materials were performed in a nitrogen atmosphere at T_{max} = 1600, 1700, 1800, or 2000 °C using graphite crucibles in a graphite furnace (heating rates, 10 °C/min (25–1400 °C) and 2 °C/min (1400–T_{max}), dwell time 3 h). The samples were subsequently powdered in a WC ball mill and analysed with a Siemens D5000/Kristalloflex (Cu-$K_{\alpha1}$ radiation) equipped with a position sensitive detector and a quartz primary monochromator.

2.3. Oxidation experiments

Oxidation experiments were carried out in the vertical Al_2O_3 tube furnace of a thermobalance (Bähr STA502) using an Al_2O_3 platform as a sample holder. The heating rate was 20 °C/min up to maximum temperatures of

1100, 1300, and 1500 °C, respectively. Dwell times ranged from 5 to 100 h. All experiments were carried out in flowing oxygen, which was dried by passing it over P_2O_5 powder prior to introduction into the furnace.

For first oxidation experiments, ceramic particles were used, which were prepared by simple thermolysis of the unprocessed precursor. These particles had sponge-like structures with large open pores. With an average size of less than 1 mm^3, ceramic particles of **1c** and **2c** were too small for oxidation experiments. Therefore, only samples of the aluminium-poorest composition **3c** could be used. Due to the irregular shapes of the ceramic particles, contact areas between samples and Al_2O_3 sample holder were nearly point-like and contamination, during long-term experiments at high temperatures, could be largely avoided.

It turned out to be impossible to determine the thickness of oxide scales on ceramic particles. Therefore, additional experiments were carried out at 1500 °C using warm-pressed **3c** bodies, which are marked by the index "wp" in the following. The disc-shaped samples were polished on one side. For oxidation experiments, fragments of the discs were leaned on **3c** ceramic particles, whereby the contact area to the sample holder was again minimized.

Prior to oxidation, all samples were cleaned in an ultrasonic bath in acetone for 10 min and subsequently dried. The phase content of starting material and oxidized samples was determined using micro Raman spectroscopy (LABRAM, Dilor, excitation wave length 488 nm). All samples were weighed prior to and after oxidation (Ultramicro, Sartorius, resolution 0.0001 mg). SEM investigations were carried out using a Zeiss DSM 962.

3. Results and discussion

3.1. Precursor synthesis

The reaction of boron-free oligosilazanes, namely $[Me_2SiNH]_n$ ($n = 3$, 4), with $H_3Al{\cdot}NMe_3$ was recently described by Fooken et al.[15] For the synthesis of Si/B/C/N/Al precursors, we used the polymer T2(1), $[B(C_2H_4Si(CH_3)NH)_3]_n$, as starting material. This polymer consists of silazane rings of different sizes with Si atoms additionally linked by $B(C_2H_4)_3$ units. According to the literature, it was obtained by reaction of $B[(C_2H_4)Si(CH_3)Cl_2]_3$ with ammonia, though in toluene solution.[6] The produced NH_4Cl was removed by filtration. The solvent was partly distilled off to yield a T2(1) concentration of about 12 wt.%. This solution was then reacted with $H_3Al{\cdot}NMe_3$ in toluene at room temperature in different stoichiometric amounts whereby moderate gas evolution occurred. The corresponding equation is shown in Scheme 1.

The reaction proceeds via dehydrocoupling of Al–H and N–H units resulting in the formation of Al–N bonds. After the first reaction step depicted in Scheme 1, cross-linking reactions by dehydrocoupling of the $NAlH_2$ unit with further H–N groups may occur either in solution or during thermolysis.

The stoichiometric ratios used were $[B(C_2H_4Si(CH_3)NH)_3]:[H_3Al{\cdot}NMe_3] = 3{:}3$, 3:2, or 3:1. In the first case, one formula unit of the polyborosilazane having three NH groups, complete reaction with one AlH_3 unit should lead to the formation of AlN_3 centres accompanied by evaporation of three molecules H_2. With a lower amount of $H_3Al{\cdot}NMe_3$, NH groups will remain unreacted within the molecules.

However, the IR spectra of polymers **1**–**3** all revealed the presence of N–H and Al–H groups by vibration bands at 3375 cm^{-1} (ν N–H) and 1853 cm^{-1} (ν Al–H). The relative intensity of the N–H vibration absorption slightly decreased when the aluminium content is increased whereas Al–H vibration bands appeared to be more intense in Al-rich polymers. We therefore assume that only one or two of the three H atoms present in "AlH_3" react with N–H at low temperatures ($\leqslant 120$ °C). During thermolysis though, the reactivity of residual functional groups (Al–H and N–H) will most probably favour further cross-linking reactions thus enhancing the ceramic yield.

Furthermore, the IR spectra of the as-obtained polymers signalled the presence of Si–H groups. The intensity of this absorption at about 2100 cm^{-1} increased with increasing Al content. The formation of Si–H units within the polymer can be explained by a ring opening reaction caused by electrophilic attack of the alane on the nitrogen atoms of eight-membered silazane rings which are present in T2(1).[15]

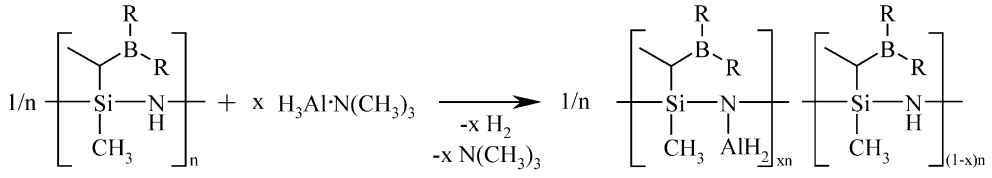

Scheme 1.

3.2. Ceramization of the polymers

The organometallic polymers **1**–**3** were transformed into ceramic particles by heating to 1400 °C in an argon atmosphere. The mass loss during this transformation was measured by thermogravimetric analysis (TGA, heating rate 5 °C/min). The results are shown in Fig. 1. For comparison, the TGA curve of the Al-free starting polymer T2(1) is inserted.

During thermolysis of T2(1), depolymerization reactions occurred leading to evaporation of small silicon-containing molecules. Consequently, the ceramic yield at 1400 °C was very low (55%). By addition of $H_3Al{\cdot}NMe_3$ to T2(1) solutions, T2(1) units can be cross-linked with formation of N–AlH–N or AlN_3 units resulting in a significantly increased molecular weight.

In these molecules, depolymerization is less probable. With an Al content of 3.6 wt.% in **3**, the ceramic yield amounted to 63% whereas an Al concentration of 6.4 wt.% in **2** led to a ceramic yield of 70%. Further increase of the Al content to 9.2 wt.% in **1** did not strongly affect the ceramic yield (71%). We therefore assume that addition of a higher amount of aluminium (>9.2 wt.%) will not produce further cross-linking.

Thermolysis of T2(1) is characterized by three decomposition steps starting at about 100, 280, and 400 °C. These steps were also present in the TGA curve of Al-poor material **3** whereas decomposition of Al-rich **1** occurred in two steps. Although three steps were observed during decomposition of polymer **2**, the TGA curves of **2** and **1** were very similar.

Table 1
Polymer composition (wt.%)

	Si	C	H	N	B	Al	O	Formula
1	28.0	38.1	7.7	14.4	3.3	9.2	0.9	$SiC_{3.2}H_{7.7}N_{1.0}B_{0.31}Al_{0.34}$
2	27.4	40.1	7.8	14.8	3.4	6.4	1.0	$SiC_{3.4}H_{7.9}N_{1.1}B_{0.32}Al_{0.24}$
3	26.4	40.7	8.1	15.1	3.6	3.6	1.5	$SiC_{3.6}H_{8.3}N_{1.1}B_{0.35}Al_{0.14}$

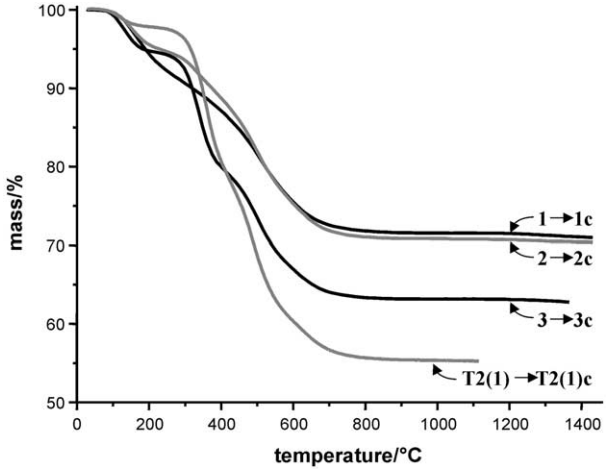

Fig. 1. TGA of polymers **1**–**3** and T2(1) (heating rate, 5 °C/min; Ar atmosphere).

During thermolysis, the polymers **1**–**3** were transformed into black hard ceramic materials, which are denoted in the following as **1c**–**3c**. Ceramic particles contained large open pores causing a sponge-like structure. Their shape was comparable to that observed for similar materials obtained by thermolysis of unprocessed Si/B/C/N/H polymers.[10] Elemental compositions of the as-thermolysed materials **1c**–**3c** are given in Table 2. Hydrogen atoms were not detected within the materials (<0.1 wt.%). Compared to the compositions of the respective polymers (see Table 1), the carbon content of the ceramics was significantly reduced by about 50 at.% whereas the Si:N:B:Al atomic ratio remained almost constant during thermolysis. The main difference between the compositions of **1c**, **2c**, and **3c** was the decreasing aluminium content of 11.3 wt.% in **1c**, 7.3 wt.% in **2c**, and 4.6 wt.% in **3c**.

3.3. High temperature behaviour

The high temperature mass stability of as-obtained ceramics **1c–3c** was investigated by high temperature thermogravimetric analysis (HT-TGA) in an argon atmosphere up to 2150 °C with a heating rate of 5 °C/min. The results are shown in Fig. 2. The HT-TGA curve of T2(1)-derived material T2(1)c is inserted.

The ceramic material derived from T2(1) is high temperature stable in an argon atmosphere. Up to 1800 °C, no mass loss was detected. At higher temperatures, a slow but continuously increasing mass loss occurred leading to a mass reduction of 1.8 wt.% at 2000 °C and 5.3 wt.% at 2150 °C. The presence of aluminium in materials **1c–3c** caused a deterioration of the high temperature mass stability compared to T2(1)c. Amazingly, the Al content was not linearly correlated to the mass loss during the experiment. Material **3c** with the lowest Al concentration was only slightly more stable than material **1c** with the highest Al concentration, whereas ceramic **2c** started to decompose at relatively low temperatures.

The composition of Al-poor material **3c** was almost stable up to 1880 °C (mass loss 1.2%). Between 1880 and 2000 °C, decomposition reactions were accelerated. At higher temperatures, evaporation proceeded slightly slower. The mass losses amounted to 3.0% at 2000 °C and 6.3% at 2150 °C. Ceramic **2c** lost mass already at 1450 °C with a mass reduction of 6.8% at 1880 °C. Further increase of the temperature led to accelerated decomposition in one step with a final mass loss of 19.8% at 2150 °C. This value corresponded approximately to the total nitrogen content in this material (see Table 2) indicating that Si_3N_4, BN and AlN completely

decompose during the experiment. Al-rich ceramic **1c** exhibited a continuous but slow mass loss up to 2000 °C (3.6%). At higher temperatures, decomposition proceeded faster resulting in a final mass reduction of 9.1% at 2150 °C.

Additionally, the crystallization behaviour of ceramic materials **1c**–**3c** in a nitrogen atmosphere was analysed. The as-thermolysed samples were heated to 1600, 1700, 1800, or 2000 °C. The maximum temperature was held for 3 h. The annealed samples were powdered in a WC ball mill and subsequently analysed by X-ray diffraction (XRD). The diffraction patterns of (heat treated) Al-rich **1c** and Al-poor **3c** are shown in Fig. 3. The respective diagrams of material **2c** are omitted because they are very similar to those of **3c** up to 1800 °C.

The as-thermolysed materials contained nano-sized SiC crystals causing broad reflections at about 35.8, 60.6, and 72.1 °. These signals were clearly more distinct in the diagram of **1c** showing an advanced state of crystallinity in the Al-rich material. Furthermore, two very broad reflections at about 26 and 42 ° were detected in the diagrams of both materials. They are usually attributed to a turbostratic BNC_x phase in Si/B/C/N ceramics. Heat treatment at 1600 °C led to a distinct signal sharpening in both materials. Here again, the reflections of material **1c** were significantly sharper than those of **3c**. Whereas the diagram of **1c** shows three distinguishable SiC signals in the 30–40 ° region, these reflections are still very broad in the diagram of **3c**. During annealing at 1700 °C, SiC crystallization in material **1c** proceeded leading to an increased intensity of the reflection peaks. Furthermore, broad reflections of a second crystalline phase were detected in low intensity. They can be assigned to AlN, 2h–SiC or to the mixed phase $(AlN)_x(SiC)_{1-x}$ since the reflection patterns of all three phases are very similar. In contrast to this, heat treated **3c** contained β-Si_3N_4 and AlN(+SiC) crystals besides SiC. At 1800 °C, both materials **1c** and **3c** seemed to be composed of crystalline α/β-SiC, β-Si_3N_4, AlN(+SiC), and a turbostratic BNC_x phase. The amount of crystallized Si_3N_4, however, was significantly smaller in **1c** than in **3c**. Heat treatment at 2000 °C led to a decrease of the Si_3N_4 signal intensities in both diagrams compared to the 1800 °C diagrams. Crystalline Si_3N_4 is not stable at this temperature and decomposes releasing nitrogen gas. Beside small amounts of residual Si_3N_4, the 2000 °C diagrams revealed the presence of crystalline SiC and AlN(+SiC). Whereas the intensity of Si_3N_4 reflections was clearly smaller in **1c** than in **3c**, AlN(+SiC) signals were more intense in Al-rich **1c**. Remarkably, the diffraction patterns of **2c** annealed at 2000 °C (not shown here) revealed the complete absence of crystalline Si_3N_4 even though the XRD diagrams of **2c** and **3c** are very similar up to 1800 °C and the Si_3N_4 content in **2c** should be higher than in **1c**. In all materials the very broad reflections of the BNC_x phase were only marginally affected by the heat treatments. The maximum was slightly shifted to higher 2θ values at higher temperatures.

The differences observed in the XRD patterns of ceramics **1c**–**3c** are probably related to the variation of

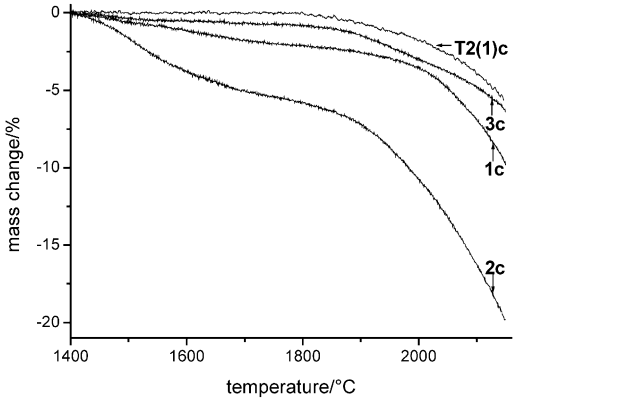

Fig. 2. High temperature TGA of ceramics **1c**–**3c** and T2(1)c (1400–2150 °C, heating rate, 5 °C/min, Ar atmosphere).

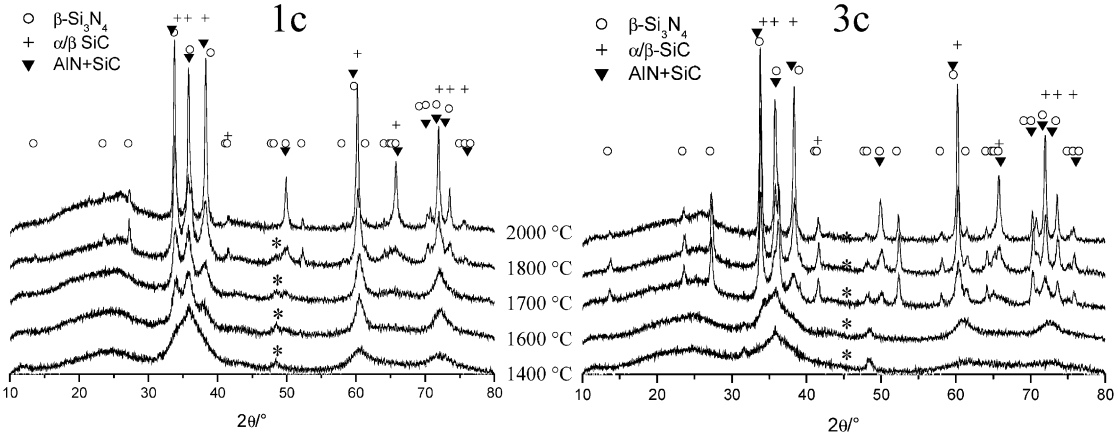

Fig. 3. XRD diagrams of as-thermolysed and annealed **1c** and **3c** (annealing time, 3 h; N_2 atmosphere). WC reflections due to the preparation technique are marked by an asterisk *.

Table 2
Composition of ceramic materials (wt.%, at.% in parenthesis, standardized to 100%)

	Si	C	N	B	Al	O	Formula
1c	37.5 (22.6)	26.0 (36.7)	20.6 (24.9)	4.8 (7.5)	11.3 (7.1)	1.0 (1.0)	$SiC_{1.6}N_{1.1}B_{0.33}Al_{0.31}$
2c	37.8 (23.2)	25.9 (37.2)	20.4 (25.1)	4.8 (7.7)	7.3 (4.7)	1.9 (2.1)	$SiC_{1.6}N_{1.1}B_{0.33}Al_{0.20}$
3c	37.2 (23.0)	26.0 (37.5)	21.1 (26.1)	5.3 (8.5)	4.6 (3.0)	1.8 (2.0)	$SiC_{1.6}N_{1.1}B_{0.37}Al_{0.13}$

chemical composition i.e. the decreasing aluminium content from 11.3 wt.% in **1c** to 4.6 wt.% in **3c**. A higher amount of aluminium seems to support SiC crystallization at lower temperatures whereas it retards Si_3N_4 crystallization at higher temperatures. Despite of the higher Al content in material **1c** compared to **3c**, AlN(+SiC) crystallization seemed to be more pronounced in Al-poor material **3c** up to 1800 °C. At 2000 °C though, the intensity of AlN+SiC reflections was highest in Al-rich **1c**. The amount of crystalline silicon nitride formed in heat treated samples decreased with increasing Al content. This is due to the fact, that nitrogen atoms are preferably bonded to boron or aluminium atoms thus reducing the number of N atoms available for the formation of Si_3N_4.

3.4. Oxidation experiments

Weight change measurements as a function of oxidation time and temperature can provide an indication of the whereabouts of boron. Assuming that **3c** is oxidized according to its nominal phase content, Eq. (1) can be used to calculate the mass change per formula unit during oxidation.

$$Si_uAl_vB_wC_xN_y + (u + 3/4v + 3/4w + x/2)O_2 \rightarrow uSiO_2 + v/2Al_2O_3 + w/2B_2O_3 + CO\uparrow + 2N_2\uparrow \quad (1)$$

Incorporation of the total boron content into the scale would lead to a mass increase of 13%/formula unit. Complete volatilisation of boron as B_2O_3 would result in a mass loss of 5%.

Mass changes measured after oxidation of **3c** and $\mathbf{3c}_{WP}$ are shown in Fig. 4. At 1100 °C and 1300 °C, ceramic particles showed a mass gain increasing with time and temperature. Due to the unknown surface area of the samples the mass changes could not be normalized to unit area. However, the distinct mass increases indicated that at least part of the boron was incorporated into the scales at these temperatures. At 1500 °C, mass gain with time was less pronounced and slightly lower than at 1300 °C. After long-term oxidation at 1500 °C, minor melt formation between **3c** particles and Al_2O_3 sample holder was observed. Therefore, these data have a higher uncertainty. However, a striking difference between **3c** ceramic particles and warm-pressed bodies was observed. The latter showed an increasing mass loss with increasing oxidation time at 1500 °C.

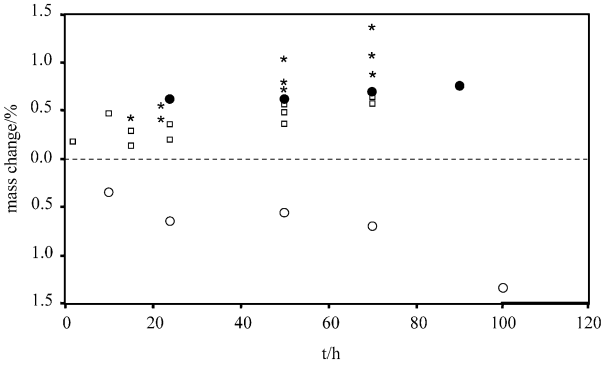

Fig. 4. Mass changes after oxidation in dry O_2 at 1100 °C (squares), 1300 °C (stars), and 1500 °C (filled circles). The open circles give results of warm-pressed bodies after oxidation at 1500 °C. Mass changes are not normalised to unit area!

SEM pictures of ceramic particles after oxidation for 100 h at 1100 °C, 1300 °C, and 1500 °C are shown in Fig. 5a–c. After 100 h at 1100 °C, despite the observed mass gain, hardly any oxide scale was to be seen on the ceramic particles (Fig. 5a). Increasing the temperature by 200 °C (Fig. 5b), the edges of the particles became apparently rounded, indicating that a dense, homogenous oxide scale formed on the whole sample. Cracking and partial spallation of the scales, which were observed after oxidation of Si/B/C/N ceramics under the same conditions, were not found.[10]

Scales remained free of cracks even after 100 h at 1500 °C (Fig. 5c). Comparison with the starting material (Fig. 5d) showed, that part of the big pores of the sponge-like structures of the ceramic particles were covered by a very thin (50 nm) oxide skin. This was in contrast to oxidation of Si/B/C/N materials, where the scales followed the surface topography of the samples without covering pores. How these oxide skins formed is not yet understood. Oxide scales grown on all ceramic particles at all temperatures were rather homogeneous and largely amorphous (see Raman spectrum **1** in Fig. 6). Deviating scale morphologies, which were sporadically observed, could be ascribed to crystallization of cristobalite and another crystalline phase, possibly mullite (**2** in Fig. 6). In contrast to Si/B/C/N ceramics, crystallization was never accompanied by bubble formation.[10]

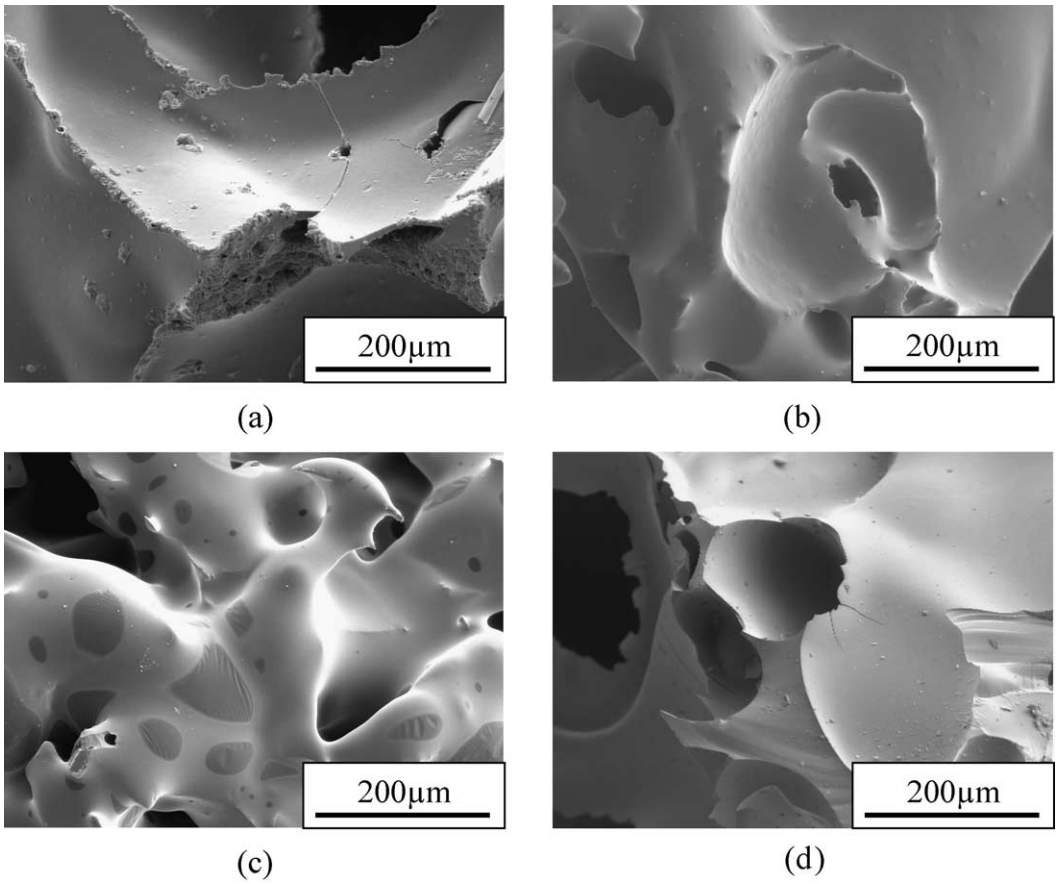

Fig. 5. Oxide scales on ceramic particles of **3c** after oxidation for 100 h at (a) 1100 °C, (b) 1300 °C, and (c) 1500 °C. An image of an as-thermolysed ceramic particle is shown for comparison (d).

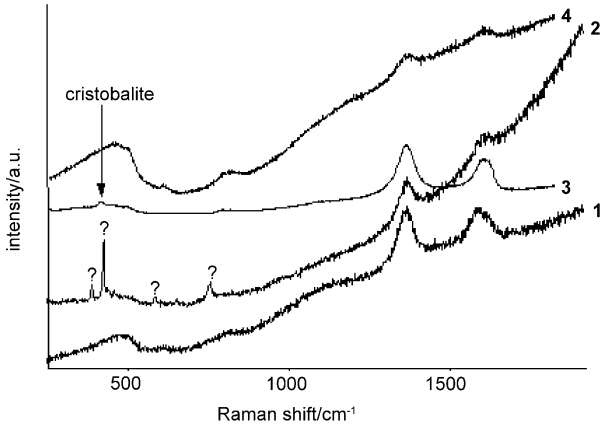

Fig. 6. Raman spectra of ceramic particles and warm-pressed bodies after oxidation at 1500 °C. The D- and G- bands of carbon at 1356 and 1600 cm^{-1} arise from the underlying substrate. **1** and **2**: scales on ceramic particles, **3** and **4** on warm-pressed materials.

Oxide scales, which formed on $\mathbf{3c}_{WP}$ during oxidation, were spatially less homogenous. Although prevailing parts of the surface area were covered by unstructured scales (top left part of Fig. 7), needle-shaped crystallites were observed in large areas (top right part of Fig. 7). A relationship between oxidation time and amount of crystalline phase was not found. However, striking differences in the underlying substrate areas were observed (bottom part of Fig. 7). While the substrate beneath the amorphous oxide (**4** in Fig. 6) scale was rather smooth, it appeared textured under the crystalline scale. It is, therefore, conceivable that inhomogeneities in the substrate microstructure have significant influence on the oxidation behaviour.

Raman spectroscopy gave cristobalite (**3** in Fig. 6) as the only crystalline phase at all oxidation times. A characteristic Raman spectrum is shown in Fig. 6.

It shall be emphasized that significant fractions of the oxide scales crystallised during oxidation without accompanying bubble formation. Moreover, both, amorphous and crystalline scales showed a perfect adhesion to the ceramic substrate.

Measurements of the oxide scale thickness were carried out in the SEM using fractured surfaces. The results are shown in Fig. 8. As can be seen, the scale growth rate on $\mathbf{3c}_{WP}$ is only slightly enhanced compared to CVD–SiC. From the cross sections shown in Fig. 7 it is evident, that the scale thickness has some variation over the sample. The value of the fitted parabolic oxidation rate constant (0.57 $\mu m^2/h$) has therefore, a high uncertainty. It is not clear, if the used parabolic

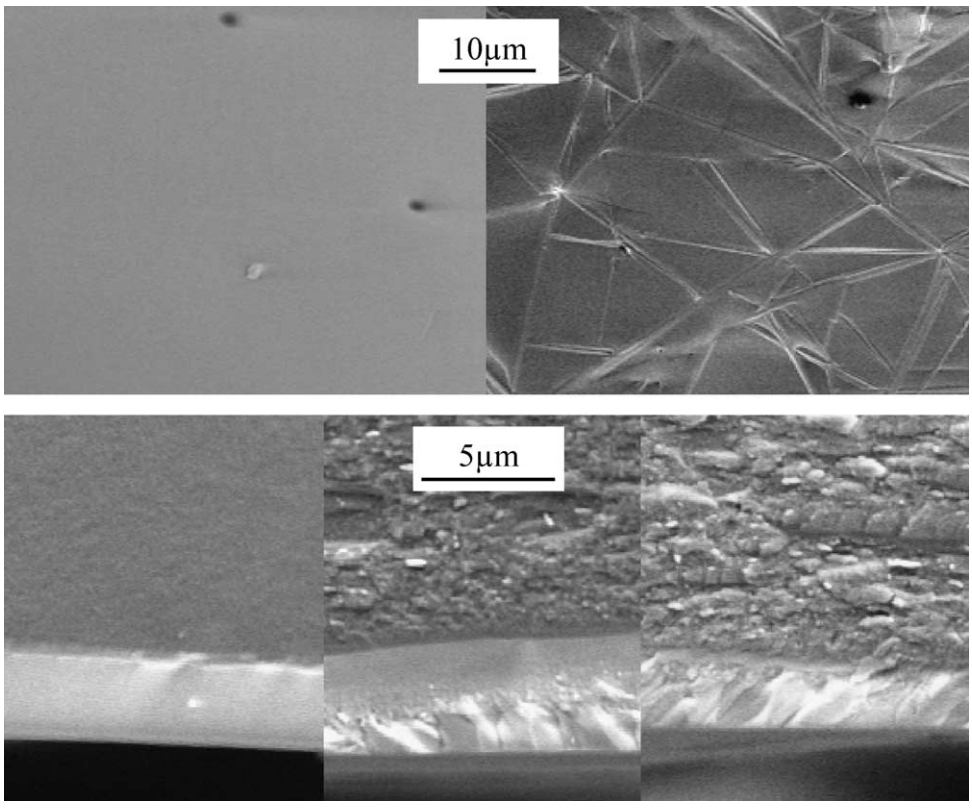

Fig. 7. Oxide scales on warm-pressed bodies (**3c**$_{WP}$) after oxidation for 10 h at 1500 °C. Top: surface views, bottom: cross sections.

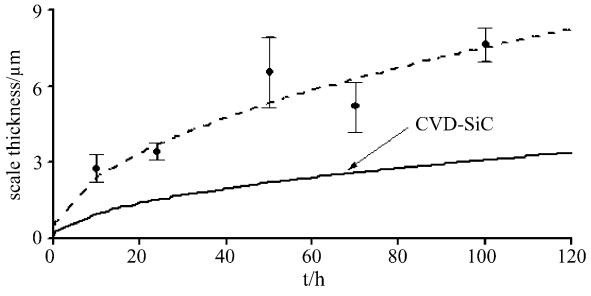

Fig. 8. Scale thickness on **3c**$_{WP}$ as a function of oxidation time at 1500 °C. The points are average values of 3–10 measurements of the scale thickness. The error bars give the standard deviation. Data for CVD–SiC are given for comparison.[11]

approximation is an adequate description for longer times.

4. Conclusions

The incorporation of aluminium into precursors for Si/B/C/N ceramics was achieved by a simple procedure. The dehydrocoupling reaction of a polyborosilazane and an alane was performed in different stoichiometric ratios to deliver Si/B/C/N/Al precursors with adjustable aluminium content. They were transformed into ceramic materials in about 63–71% yield, the mass loss decreasing with increasing Al concentration of the samples. The cross-linking of polyborosilazane units by Al atoms increased the molecular weight of the polymers and hindered depolymerization reactions. The resulting ceramic materials were predominantly amorphous after thermolysis. Crystallization was induced by heat-treatment experiments leading to the formation of a microstructure composed of crystalline SiC, Si_3N_4, AlN (or a mixed phase AlN + SiC) and a matrix phase which most probably is composed of turbostratic BNC_x layers. In comparison with the high temperature stability of the corresponding Al-free materials, Si/B/C/N/Al ceramics are less stable. However, this effect may be negligible when only small amounts of aluminium are present. The addition of aluminium had a beneficial effect on the oxidation behaviour of the precursor-derived ceramics. Cracking and spallation of the oxide scales, which are a general problem during the high temperature oxidation of Si/(B)/C/N ceramics, could be entirely impeded.[16] With scale growth rates comparable to CVD–SiC and CVD–Si_3N_4, Si/B/C/N/Al precursor-derived ceramics are, therefore, promising candidates for high-temperature applications in oxidizing environments. Future work will focus on the relationship between the aluminium content and the oxidation resistance.

Acknowledgements

The authors would like to thank Gerhard Kaiser (microanalytic investigations), Horst Kummer (high temperature thermogravimetric analysis), Martina Thomas (XRD measurements), and Elke Nadler (SEM). Financial support by the Deutsche Forschungsgemeinschaft (DFG) is gratefully acknowledged.

References

1. Weinmann, M., Schuhmacher, J., Kummer, H., Prinz, S., Peng, J., Seifert, H. J., Christ, M., Müller, K., Bill, J. and Aldinger, F., Synthesis and thermal behavior of novel Si–B–C–N ceramic precursors. *Chem. Mater.*, 2000, **12**, 623–632.
2. Bill, J., Kamphowe, T. W., Müller, A., Wichmann, T., Zern, A., Jalowiecki, A., Mayer, J., Weinmann, M., Schuhmacher, J., Müller, K., Peng, J., Seifert, H. and Aldinger, F., Precursor-derived Si-(B-)C-N ceramics: thermolysis, amorphous state and crystallization. *Appl. Organometal. Chem.*, 2001, **15**, 777–793.
3. Zern, A., Mayer, J., Janakiraman, N., Weinmann, M., Bill, J. and Rühle, M., Quantitative EFTEM study of precursor-derived Si–B–C–N ceramics. *J. Eur. Ceram. Soc.*, 2002, **22**, 1621–1629.
4. Müller, A., Zern, A., Gerstel, P., Bill, J. and Aldinger, F., Boron-modified poly(propenylsilazene)-derived Si–B–C–N ceramics: preparation and high temperature properties. *J. Eur. Ceram. Soc.*, 2002, **22**, 1631–1643.
5. Baldus, H. P., Wagner, O. and Jansen, M., Synthesis of advanced ceramics in the system Si–B–N and Si–B–N–C employing novel presursor compounds. *Mat. Res. Soc. Symp. Proc*, 1992, **271**, 821–826.
6. Riedel, R., Kienzle, A., Dreβler, W., Ruwisch, L., Bill, J. and Aldinger, F., A silicoboron carbonitride ceramic stable to 2000 °C. *Nature*, 1996, **382**, 796–798.
7. Heimann, D., *Oxidationsschutzschichten für kohlefaserverstärkte Verbundwerkstoffe durch Polymer-Pyrolyse*. PhD thesis, 1996, Universität Stuttgart.
8. Aldinger, F., Weinmann, M. and Bill, J., Precursor-derived Si–B–C–N ceramics. *Pure & Appl. Chem.*, 1998, **70**, 439–448.
9. Weinmann, M., Kamphowe, T. W., Schuhmacher, J., Müller, K. and Aldinger, F., Design of polymeric Si–B–C–N ceramic precursors for application in fiber-reinforced composite materials. *Chem. Mater.*, 2000, **12**, 2112–2122.
10. Butchereit, E., Nickel, K. G. and Müller, A., Precursor derived Si–B–C–N ceramics: oxidation kinetics. *J. Am. Ceram. Soc.*, 2001, **84**, 2184–2188.
11. Ogbuji, L. U. J. T. and Opila, E. J., A comparison of the oxidation kinetics of SiC and Si_3N_4. *J. Electrochem. Soc.*, 1995, **142**, 925–930.
12. Gogotsi, Y. G., Yaroshenko, V. P. and Portz, F., Oxidation resistance of boron carbide-based ceramics. *J. Mater. Sci. Letters*, 1992, **11**, 308–310.
13. Schumacher, C., *Oxidationsverhalten von Bor und Kohlenstoff beinhaltenden gesinterten Siliciumcarbid-Werkstoffen bei 1500 °C*. PhD thesis, 2001, Universität Tübingen.
14. Ruff, J. K. and Hawthorne, M. F., The amine complexes of aluminium hydride. I. *J. Am. Chem. Soc.*, 1960, **82**, 2141–2144.
15. Fooken, U., Khan, M. A. and Wehmschulte, R. J., Novel aluminium hydride derivatives from the reaction of $H_3Al{\cdot}NMe_3$ with the cyclosilazanes $[Me_2SiNH]_3$ and $[Me_2SiNH]_4$. *Inorg. Chem.*, 2001, **40**, 1316–1322.
16. Narushima, T., Lin, R. Y., Iguchi, Y. and Hirai, T., Oxidation of chemically vapor-deposited silicon nitride in dry oxygen at 1923 to 2003 K. *J. Am. Ceram. Soc.*, 1993, **76**, 1047–1051.